Non-orthogonal cracks in a smeared finite element model

R. de Borst and P. Nauta
Institute TNO for Building Materials and Building Structures, Software Engineering Department (Section DIANA), PO Box 49, 2600 AA Delft, The Netherlands
(Received November 1984; revised January 1985)

ABSTRACT

A new model for handling non-orthogonal cracks within the smeared crack concept is described. It is based on a decomposition of the total strain increment into a concrete and into a crack strain increment. This decomposition also permits a proper combination of crack formation with other non-linear phenomena such as plasticity and creep and with thermal effects and shrinkage. Relations are elaborated with some other crack models that are currently used for the analysis of concrete structures. The model is applied to some problems involving shear failures of reinforced concrete structures such as a moderately deep beam and an axisymmetric slab. The latter example is also of interest in that it confirms statements that 'reduced integration' is not reliable for problems involving crack formation and in that it supports the assertion that identifying numerical divergence with structural failure may be highly misleading.

INTRODUCTION

The formation of cracks is undoubtedly one of the most important non-linear phenomena which govern the behaviour of concrete structures. Consequently, any numerical program which is to be used for the analysis of concrete structures should embody a sound numerical procedure that handles the formation (and eventually closing and reopening) of cracks. Indeed, ever since the finite element method has been applied to concrete, the formation of cracks has received much attention.

Ngo and Scordelis[1] were probably the first to allow cracks to be formed in a finite element mesh. Cracks were allowed to propagate along predefined inter-element boundaries. Nilson[2] allowed crack propagation by disconnecting nodes if the tensile force in that particular node had exceeded a threshold value. In recent years, this so-called discrete crack approach was refined by Saouma and Ingraffea[3] and by Grootenboer[4] who developed discrete crack models in which the cracks are no longer forced to align with the original inter-element boundaries.

A major disadvantage that adheres to the discrete crack approach is the fact that the topology of the finite element mesh is changed continuously. This seems to limit the scope of the approach to research applications as in practical situations such concepts are rather unwieldy. The so-called smeared crack models[5] are more promising in this respect. In these models the formation of cracks is simulated by replacing the isotropic stiffness matrix by an orthotropic stiffness matrix upon crack formation.

In the early days of the smeared crack approach the method seemed to be inferior to the discrete crack models as somewhat irregular and often excessively diffused crack patterns were obtained. However, the introduction of a shear retention factor[6] to model dowel action and aggregate interlock and especially the replacement of the sudden drop in tensile stress after crack formation by more advanced tension-softening models[7,8] have enhanced the capabilities of smeared crack models significantly. At present, smeared crack models have evolved so far that even detailed crack propagation analyses of concrete specimens can be undertaken successfully[9].

Nevertheless, a number of questions are still unresolved and reliable answers cannot always be obtained for some important cases such as shear failures in beams and slabs. A major problem that adheres to many smeared crack models becomes apparent when we analyse such structures, namely the rotation of the principal stress axes after crack formation. In most existing smeared crack models the crack direction is fixed upon formation of a crack. Owing to aggregate interlock and dowel action as represented by a non-zero shear retention factor, shear tractions develop on the faces of the crack at continued loading, so that the principal stress directions no longer align with the crack directions. Moreover, owing to high shear stresses the major principal tensile stress may well become larger than the tensile strength, which may result in incorrect predictions of the structural behaviour. Until recently this problem has received surprisingly little attention in literature. It is mentioned, though, by Cope[10,11] who proposed to change the material axes when the stress rotation had exceeded a certain threshold angle. Obviously, this solution is not correct from a thermodynamical point of view for the same reason as non-linear orthotropic elasticity models violate thermodynamics principles[12,13]. Despite this objection, it has been shown that such a 'rotating crack' model may yield answers which are significantly better than results that are obtained by the traditional fixed crack model[14].

The authors have recently proposed another solution to this problem[15]. In the proposed algorithm a second crack is allowed to form after the change in principal stress directions has exceeded a certain threshold value, say 30° or 45°. If on subsequent loading a further rotation in principal stress directions would occur, even a third crack is allowed to occur. This procedure of allowing non-orthogonal cracks differs significantly from the procedures adopted by most other analysts. For two-dimensional stress states they mostly either allow a secondary crack to form only perpendicular to a primary crack, or assume that upon formation of a second crack all stiffness is lost[16]. Notable exceptions are the models by Litton[17], Kristjansson[18,39] and Ebbinghaus[19], but their models have rather limited capabilities in describing the force–displacement (or in smeared crack terminology the stress–strain) relation in a crack, whereas our treatment allows incorporation of the full stress–strain relation.

Another problem with smeared crack models is that the situation in which cracking and non-linear behaviour under compressive stresses occur simultaneously in an integration point cannot be handled well. Indeed, inserting the orthotropic cracked stiffness matrix in an elastoplastic stress–strain law may result in a stress state

0264–4401/85/010035–12$2.00

which neither complies with the yield function nor satisfies the fracture function. It therefore seems of vital importance to make a clear distinction between the concrete strains and the crack strains. Such a decomposition permits the development of an algorithm which yields a stress state which satisfies both the yield function and the fracture function.

A further aspect to which we will draw attention is the ability of the finite element method to correctly predict failure loads and post-failure behaviour of concrete structures. In practice, structural failure is often associated with a divergence of the iterative procedure. It is the authors' opinion that this is not correct as such a divergence may be caused by a variety of reasons, ranging from an attempt to analyse snap-back behaviour under displacement control to ordinary program errors, and we will show a typical example thereof. Hence, there is a great need for methods which permit tracing the post-peak behaviour of concrete structures so that the complete load–deformation response can be obtained, thus allowing for a proper assessment of the peak and eventually of the residual strength of concrete structures.

SMEARED CRACK MODEL FOR NON-ORTHOGONAL CRACKS

A fundamental feature of the proposed crack model is a decomposition of the total crack strain increment into a concrete strain increment $\Delta\boldsymbol{\varepsilon}^{co}$ and into a crack strain increment $\Delta\boldsymbol{\varepsilon}^{cr}$:

$$\Delta\boldsymbol{\varepsilon} = \Delta\boldsymbol{\varepsilon}^{cr} + \Delta\boldsymbol{\varepsilon}^{co} \tag{1}$$

Such a decomposition is not new and has also been advocated by other researchers[17,20]. Moreover, a similar decomposition, namely into an elastic and into a plastic strain increment is also assumed in elastoplasticity. Indeed, the final equation which we will derive for the cracked concrete bears some resemblance to the elasto-plastic stiffness matrix.

Considering the crack strain increment $\Delta\boldsymbol{\varepsilon}^{cr}$ first, we observe that this strain increment is composed of the contributions of the individual crack strain increments of a particular integration point. If we denote the vector which assembles the individual crack strain increments by $\Delta\mathbf{e}^{cr}$, we have:

$$\Delta\mathbf{e}^{cr} = (\Delta e_1^{cr}\ \Delta\gamma_1^{cr}\ \Delta e_2^{cr}\ \Delta\gamma_2^{cr} \cdots \Delta e_n^{cr}\ \Delta\gamma_n^{cr})^T \tag{2a}$$

where the superscript T denotes a transpose. Δe_n^{cr} and $\Delta\gamma_n^{cr}$ are the normal and the shear crack strain increment respectively of crack number n. The size of the vector $\Delta\mathbf{e}^{cr}$ depends on the number of open cracks in an integration point. For one open crack (2a) reduces to:

$$\Delta\mathbf{e}^{cr} = (\Delta e_1^{cr}\ \Delta\gamma_1^{cr})^T \tag{2b}$$

For each subsequent open crack in an integration point, $\Delta\mathbf{e}^{cr}$ is enlarged by two components, namely the normal and the shear crack strain of that crack.

The relation between the global crack strain increment $\Delta\boldsymbol{\varepsilon}^{cr}$ and the vector $\Delta\mathbf{e}^{cr}$ which assembles the individual crack strain increments, is given by the identity:

$$\Delta\boldsymbol{\varepsilon}^{cr} = \mathbf{N}\,\Delta\mathbf{e}^{cr} \tag{3}$$

For a two-dimensional solid, the matrix $\mathbf{N}$ reads:

$$\mathbf{N} = \begin{bmatrix} \cos^2\theta_1 & -\sin\theta_1\cos\theta_1 & \cdots & \cos^2\theta_n & -\sin\theta_n\cos\theta_n \\ \sin^2\theta_1 & \sin\theta_1\cos\theta_1 & \cdots & \sin^2\theta_n & \sin\theta_n\cos\theta_n \\ 2\sin\theta_1\cos\theta_1 & \cos^2\theta_1-\sin^2\theta_1 & \cdots & 2\sin\theta_n\cos\theta_n & \cos^2\theta_n-\sin^2\theta_n \end{bmatrix} \tag{4}$$

where θ_n is the inclination angle of the normal of crack number n with the x-axis. As $\Delta\mathbf{e}^{cr}$ has a variable length depending on the number of open cracks, the size of the transformation matrix $\mathbf{N}$ also depends on the number of open cracks. For one open crack $\mathbf{N}$ is a 3*2 matrix, for 2 open cracks $\mathbf{N}$ is a 3*4 matrix and so on.

In a similar way, we may develop a relation between the global stress increment $\Delta\boldsymbol{\sigma}$ and the stress increments in the cracks. When we define

$$\Delta\mathbf{s}^{cr} = (\Delta s_1^{cr}\ \Delta t_1^{cr}\ \Delta s_2^{cr}\ \Delta t_2^{cr} \cdots \Delta s_n^{cr}\ \Delta t_n^{cr})^T \tag{5}$$

as the vector which contains the stress increments in the cracks (Δs_n^{cr} being the normal and Δt_n^{cr} being the shear stress increment in crack number n), we can derive:

$$\Delta\mathbf{s}^{cr} = \mathbf{N}^T\,\Delta\boldsymbol{\sigma} \tag{6}$$

The transformation matrix $\mathbf{N}$ is again defined by (4).

To complete our system of equations, we need a constitutive relation for the intact concrete and a stress–strain law for the smeared cracks. For the concrete between the cracks we assume an incrementally linear constitutive relationship:

$$\Delta\boldsymbol{\sigma} = \mathbf{D}^{co}\,\Delta\boldsymbol{\varepsilon}^{co} \tag{7}$$

where the matrix $\mathbf{D}^{co}$ contains the constitutive properties of the uncracked concrete. Linearized endochronic, elastic-plastic or fracturing models may for instance be used to formulate this matrix. In the sample problems which we will discuss, we have employed a simple elastic–perfectly plastic model.

Similarly to the stress–strain relation for the concrete (7), we can define a relation between the crack strain increment $\Delta\mathbf{e}^{cr}$ and the crack stress increment $\Delta\mathbf{s}^{cr}$:

$$\Delta\mathbf{s}^{cr} = \mathbf{D}^{cr}\,\Delta\mathbf{e}^{cr} \tag{8}$$

The structure of the matrix $\mathbf{D}^{cr}$ is slightly more complicated than that of the stress–strain matrix $\mathbf{D}^{co}$ because the size of $\mathbf{D}^{cr}$ depends on the number of open cracks in an integration point. For one crack it is a 2*2 matrix, for two cracks it is a 4*4 matrix and so on. For n open cracks we can write formally:

$$\mathbf{D}^{cr} = \begin{bmatrix} \mathbf{D}_1^{cr} & \mathbf{0} & \mathbf{0} \\ \mathbf{0} & \mathbf{D}_2^{cr} & \mathbf{0} \\ \mathbf{0} & \mathbf{0} & \mathbf{D}_n^{cr} \end{bmatrix} \tag{9}$$

All the off-diagonal 2*2 submatrices are zero and this implies that no coupling effects between different cracks are considered. The stress increment in crack n is assumed to depend on the crack strain increment of the same crack only, their relation being given by the 2*2 submatrix $\mathbf{D}_n^{cr}$. This may be a simplification of reality, as the amount of damage which has already been done in an existing crack reduces the energy that can be released in subsequent cracks.

In addition to the idealization that the off-diagonal

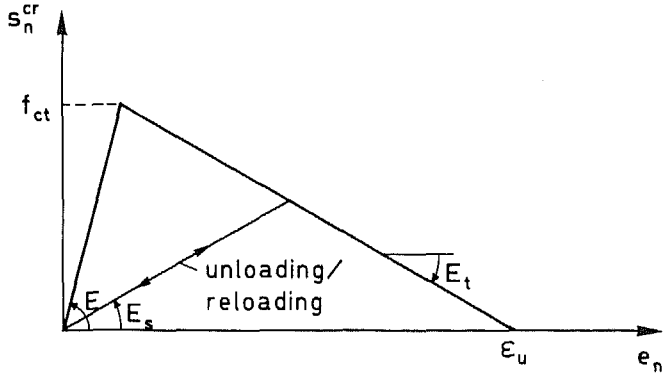

Figure 1 Normal stress *versus* normal strain of cracked concrete

submatrices in the constitutive matrix $\mathbf{D}^{cr}$ are zero, we have also assumed that the off-diagonal terms in each submatrix $\mathbf{D}_n^{cr}$ are zero. This assumption implies that no coupling is taken into account between the normal stress increment in a crack and the shear strain increment, or between the shear stress increment and the normal strain increment. This assumption results from the consideration that it is not sensible to use very advanced models if we cannot put simpler models into practice. From *Figure 1* we read that in case of one crack the relation between the normal stress increment Δs_n^{cr} in the crack and the normal strain increment Δe_n of the cracked concrete is given by E_t, the modulus of the softening branch. The relation between increment Δs_n^{cr} and the normal strain increment of the crack Δe_n^{cr} can then be worked out to be $EE_t/(E-E_t)$ with E the Young's modulus of the uncracked concrete. We further assume that the shear strain increment $\Delta\gamma_n^{cr}$ of crack n and the shear stress increment Δt_n^{cr} of that crack are related through $\frac{1}{2}\beta E/[(1-\beta)(1+\nu)]$, where ν is Poisson's ratio and β is the so-called shear retention factor[6]. The stiffness $\frac{1}{2}\beta E/[(1-\beta)(1+\nu)]$ derives from the decomposition of the total shear strain increment into a concrete and into a crack shear strain increment. With the above relation our approach can be connected with the more traditional approaches which assume a relation $\frac{1}{2}\beta E/(1+\nu)$ between the total shear strain increment and the shear stress increment. Hence, we arrive at the following constitutive relation for a crack:

$$\mathbf{D}_n^{cr}=\begin{bmatrix}\dfrac{EE_t}{E-E_t} & 0\\ 0 & \dfrac{\beta}{1-\beta}\dfrac{E}{2(1+\nu)}\end{bmatrix} \tag{10}$$

It is noted that the magnitude of E_t mainly depends on the ultimate normal strain ε_u of the softening branch, which has to be adjusted in accordance with the element size as to obtain objective results with regard to the finite element mesh. Then, the fundamental parameter which governs crack propagation is the fracture energy G_f[7-9].

With the aid of (1), (3), (6), (7) and (8) we can develop the stress–strain relation for the cracked concrete. To this end we substitute (1), (3) and (7) in (6). This gives:

$$\Delta\mathbf{s}^{cr}=\mathbf{N}^T\mathbf{D}^{co}[\Delta\boldsymbol{\varepsilon}-\mathbf{N}\,\Delta\mathbf{e}^{cr}] \tag{11}$$

Together with (8), this yields:

$$\Delta\mathbf{e}^{cr}=[\mathbf{D}^{cr}+\mathbf{N}^T\mathbf{D}^{co}\mathbf{N}]^{-1}\mathbf{N}^T\mathbf{D}^{co}\,\Delta\boldsymbol{\varepsilon} \tag{12}$$

Substituting this relation in

$$\Delta\boldsymbol{\sigma}=\mathbf{D}^{co}[\Delta\boldsymbol{\varepsilon}-\mathbf{N}\,\Delta\mathbf{e}^{cr}] \tag{13}$$

provides us with the constitutive relation for the cracked concrete:

$$\Delta\boldsymbol{\sigma}=[\mathbf{D}^{co}-\mathbf{D}^{co}\mathbf{N}(\mathbf{D}^{cr}+\mathbf{N}^T\mathbf{D}^{co}\mathbf{N})^{-1}\mathbf{N}^T\mathbf{D}^{co}]\,\Delta\boldsymbol{\varepsilon} \tag{14}$$

It is noted that as long as the constitutive matrices $\mathbf{D}^{co}$ and $\mathbf{D}^{cr}$ remain symmetric, the stress–strain matrix also remains symmetric.

CRACKING AND OTHER NON-LINEAR PHENOMENA

The behaviour of concrete under compressive triaxial stress states is very complicated. It resembles materials like rock and sand in that the strength also depends on the first stress invariant and because we also observe dilatancy and strain-softening in triaxial tests[21,22]. As we have concentrated on the numerical modelling of cracking, we have refrained from using sophisticated models for the description of the behaviour of the concrete under compressive stress states. Merely an elastic–perfectly plastic model has been used in conjunction with a Mohr–Coulomb yield locus (see *Figure 2*). Test results indicate that the angular Mohr–Coulomb yield surface is conservative and they point at a slightly more convex yield surface for concrete. The load-carrying capacity of a structure may thus be underestimated somewhat using this failure criterion. A more severe restriction is the fact that no hardening and especially no softening under compressive loading have been included in the analyses. This probably has a greater impact on the results than a yield surface which is too conservative. Another shortcoming of this plasticity model is the fact that we have used a classical associated flow rule (normality). The plastic volume expansion which is predicted by an associated flow rule when used in conjunction with a pressure-sensitive yield criterion, greatly overestimates the plastic dilation observed in triaxial tests. For confined situations which may occur in thick-walled structures, use of an associated flow rule may therefore cause a too stiff load–deformation response and may even result in an overestimation of the failure load. Future calculations should therefore include a more advanced non-associated hardening/softening model for concrete[21].

Especially with shear failures, there exist regions in the

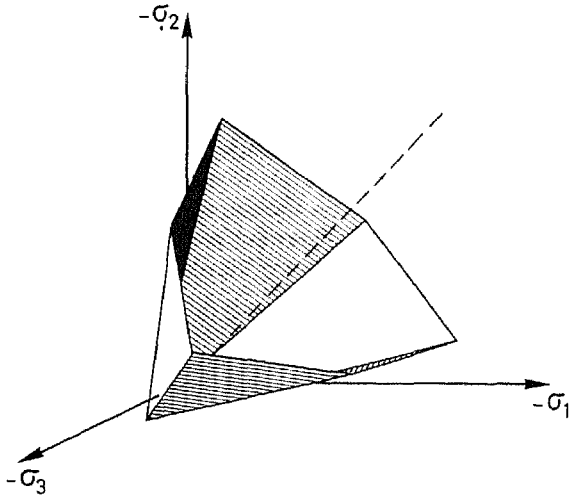

Figure 2 Mohr–Coulomb yield locus in the three-dimensional stress space

structure in which we have high compressive stresses parallel to the cracks. Numerically, this results in integration points which are not only cracked but also show plastic behaviour. As argued, the decomposition of the total strain increment into a concrete and into a crack strain increment allows for the development of an algorithm that yields a stress state which not only complies with the yield function, but also agrees with the fracture function. Yet, straightforward application of (14) generally results in a stress state lying outside of the yield surface. This is because (14) is in fact a linearization around the current stress state, and strictly speaking this equation is only exact for infinitesimal changes but not for finite strain increments. This problem of drifting from the yield surface exists whether we have crack formation or not. A number of methods have been devised that aim at minimizing or eliminating this drifting tendency. A possibility, which has been shown to be accurate for frictional materials like concrete and soils is to apply a correction $\delta\boldsymbol{\sigma}$,

$$\delta\boldsymbol{\sigma} = -\frac{f(\boldsymbol{\sigma})}{\dfrac{\partial f^{\mathrm{T}}}{\partial\boldsymbol{\sigma}}\mathbf{D}^{e}\dfrac{\partial f}{\partial\boldsymbol{\sigma}}}\mathbf{D}^{e}\frac{\partial f}{\partial\boldsymbol{\sigma}} \tag{15}$$

to the stress point[23,41], where f represents the yield function and $\mathbf{D}^e$ is the elasticity matrix. The stress state after correction, however, does not necessarily comply with the fracture criterion. Pending the development of a more sophisticated algorithm, we have applied the following procedure.

Upon violation of the tension cut-off criterion, we first determine the intersection of the stress path with the tension cut-off. The strain increment from the initial state up to the tension cut-off is considered as elastic and the remaining part of the strain increment is treated as elastic-fracturing. A first estimate of the stress increment for the latter part is made using (14). If we have no plasticity the elasticity matrix $\mathbf{D}^e$ is substituted for $\mathbf{D}^{\mathrm{co}}$ and we may proceed to the next integration point. If we have encountered plasticity during the previous loading step so that the stress in the beginning of the present step $\boldsymbol{\sigma}^0$ is on the yield locus, the classical elastoplastic matrix is substituted for $\mathbf{D}^{\mathrm{co}}$:

$$\mathbf{D}^{\mathrm{co}} = \mathbf{D}^{e} - \frac{\mathbf{D}^{e}\dfrac{\partial f}{\partial\boldsymbol{\sigma}}\dfrac{\partial f^{\mathrm{T}}}{\partial\boldsymbol{\sigma}}\mathbf{D}^{e}}{h+\dfrac{\partial f^{\mathrm{T}}}{\partial\boldsymbol{\sigma}}\mathbf{D}^{e}\dfrac{\partial f}{\partial\boldsymbol{\sigma}}} \tag{16}$$

The scalar h represents the hardening which we set equal to zero because we assume ideal-plastic behaviour. The stress state which results from application of (14) in conjunction with (16) is on the softening branch of *Figure 1*, but a drift from the yield surface may have occurred. We therefore recompute the stress increment using:

$$\Delta\boldsymbol{\sigma} = \mathbf{D}^{e}(\Delta\boldsymbol{\varepsilon} - \Delta\boldsymbol{\varepsilon}^{\mathrm{cr}}) - \frac{f(\boldsymbol{\sigma}^{t})}{\dfrac{\partial f^{\mathrm{T}}}{\partial\boldsymbol{\sigma}}\mathbf{D}^{e}\dfrac{\partial f}{\partial\boldsymbol{\sigma}}}\mathbf{D}^{e}\frac{\partial f}{\partial\boldsymbol{\sigma}} \tag{17}$$

with

$$\boldsymbol{\sigma}^{t} = \boldsymbol{\sigma}^{0} + \mathbf{D}^{e}(\Delta\boldsymbol{\varepsilon} - \Delta\boldsymbol{\varepsilon}^{\mathrm{cr}}) \tag{18}$$

The resulting stress state $\boldsymbol{\sigma}^1 = \boldsymbol{\sigma}^0 + \Delta\boldsymbol{\sigma}$ can be shown to be on the yield surface for the Mohr–Coulomb yield locus, and also for the Drucker–Prager criterion provided that this yield function is written in a particulate form[24]. The crack strain increment follows from the initial estimate using (14) and remains unaltered during this corrector step. The crack stress increment is changed by the application of (17) and consequently, the crack strain increments $\Delta\mathbf{e}^{\mathrm{cr}}$ and the crack stress increments $\Delta\mathbf{s}^{\mathrm{cr}}$ are no longer related by the crack relations (8) to (10). Conceiving the computed plastic strain increment $\Delta\boldsymbol{\varepsilon}^p$ as an initial strain increment, we may obtain an improved estimate for the stress increment using:

$$\Delta\boldsymbol{\sigma} = [\mathbf{D}^{e} - \mathbf{D}^{e}\mathbf{N}(\mathbf{D}^{\mathrm{cr}} + \mathbf{N}^{\mathrm{T}}\mathbf{D}^{e}\mathbf{N})^{-1}\mathbf{N}^{\mathrm{T}}\mathbf{D}^{e}](\Delta\boldsymbol{\varepsilon} - \Delta\boldsymbol{\varepsilon}^{p}) \tag{19}$$

which gives stress increments that are related to the crack strain increment via (8) to (10), but the total stress may now again violate the yield function.

After an initial estimate using (14) we therefore apply an inner iteration loop using (17) to (19). Our current experiences indicate that this process always converges to a stress state which complies with the yield function and which agrees with the crack relation. Convergence may be rather slow, but this is not considered a major problem as in the case of perfect plasticity the number of Gauss points in a structure which are both cracked and show plastic behaviour, is limited.

CLOSING AND OPENING OF CRACKS

In smeared crack analyses of concrete members we experience a lot of what may be referred to as spurious cracking. Here we mean that there are quite a number of sampling points which crack, but show only small crack strains. This partly causes the diffused crack pattern of smeared crack analyses. If we omit them, we often observe that only a limited number of cracks really open and lead to failure (strain-localization). Yet, these sampling points with small crack strains pose a problem as a number of them show unloading, even close and sometimes open again in a later stage of the loading process.

Unloading of cracks occurs for instance when an integration station in the neighbourhood cracks or when new cracks in the same integration point arise. For the unloading branch we have adopted a secant approach as is shown in *Figure 1*. So when a crack starts unloading, (10) is replaced by:

$$\mathbf{D}_n^{\mathrm{cr}} = \begin{bmatrix} \dfrac{EE_s}{E-E_s} & 0 \\ 0 & \dfrac{\beta}{1-\beta}\dfrac{E}{2(1+\nu)} \end{bmatrix} \tag{20}$$

where E_s is the secant modulus of the unloading branch. This assumption is too simple as in reality we may expect some residual strain upon closing of a crack[20,25,26], but our experiences indicate that this procedure is numerically stable.

When a crack fully closes, i.e. when the normal stress in the crack changes from tension into compression, the full elastic stiffness is inserted again, so that $\Delta\boldsymbol{\sigma} = \mathbf{D}^{\mathrm{co}}\,\Delta\boldsymbol{\varepsilon}$. Although upon closing of a crack, the normal strain and the normal stress both vanish in our conception, this need not be true for the shear stress and the shear strain. Consequently, these stresses and strains are considered as initial stresses and initial strains upon closing of the crack and the stress after closing formally follows from:

$$\sigma = \sigma^0 + \int \mathbf{D}^{co}\dot{\varepsilon}\,dt \tag{21a}$$

where σ^0 is the stress state that exists when the crack closes and $\dot{\varepsilon}$ is the strain-rate vector. If we have linear-elastic material behaviour in compression ($\mathbf{D}^{co}=\mathbf{D}^{e}$), (21a) reduces to:

$$\sigma = \sigma^0 + \mathbf{D}^{e}(\varepsilon - \varepsilon^0) \tag{21b}$$

with ε^0 the strain that exists in the sampling point upon closing of the crack. When a crack opens again the shear stress and the crack shear strain are initialized with the values which follow from σ^0 and ε^0, i.e. the shear stress and the shear strain which existed when the crack closed. During reloading (20) is used for the incremental relation between the crack stresses and the crack strains. If the normal strain in the crack exceeds the previously reached maximum strain, (20) is replaced by (10) for the softening branch.

RELATION WITH OTHER SMEARED CRACK MODELS

There is a clear relation between the model described here and a number of other crack models which are currently employed in finite element analyses of concrete structures. For instance, when we have only one crack and when there is no plasticity, our crack model reduces to Bažant and Oh's[7] compliance formulation. This is demonstrated most simply by considering a crack with the normal in the x-direction. This is by no means a restriction as an analysis for a crack with an arbitrary inclination angle would yield exactly the same result. For a crack with the normal aligned with the x-axis the transformation matrix $\mathbf{N}$ reads:

$$\mathbf{N} = \begin{bmatrix} 1 & 0 \\ 0 & 0 \\ 0 & 1 \end{bmatrix} \tag{22}$$

With the well-known expression

$$\mathbf{D}^{co} = \frac{E}{1-\nu^2}\begin{bmatrix} 1 & \nu & 0 \\ \nu & 1 & 0 \\ 0 & 0 & \frac{1}{2}(1-\nu) \end{bmatrix} \tag{23}$$

for the elasticity matrix in a plane stress situation, we can derive that:

$$\mathbf{N}^{T}\mathbf{D}^{co}\mathbf{N} = \frac{E}{1-\nu^2}\begin{bmatrix} 1 & 0 \\ 0 & \frac{1}{2}(1-\nu) \end{bmatrix} \tag{24}$$

Adding the stress–strain matrix $\mathbf{D}^{cr}$ for the crack (see (10)) and inverting yields:

$$(\mathbf{D}^{cr}+\mathbf{N}^{T}\mathbf{D}^{co}\mathbf{N})^{-1} = \frac{1-\nu^2}{E}\begin{bmatrix} \frac{E-E_t}{E-E_t\nu^2} & 0 \\ 0 & 2\frac{1-\beta}{1-\nu} \end{bmatrix} \tag{25}$$

Premultiplying with $\mathbf{D}^{co}\mathbf{N}$ and postmultiplying with $\mathbf{N}^{T}\mathbf{D}^{co}$ and subtracting the result from $\mathbf{D}^{co}$ yields:

$$\mathbf{D}^{co} - \mathbf{D}^{co}\mathbf{N}(\mathbf{D}^{cr}+\mathbf{N}^{T}\mathbf{D}^{co}\mathbf{N})^{-1}\mathbf{N}^{T}\mathbf{D}^{co} =$$

$$\begin{bmatrix} \frac{EE_t}{E-E_t\nu^2} & \frac{\nu EE_t}{E-E_t\nu^2} & 0 \\ \frac{\nu EE_t}{E-E_t\nu^2} & \frac{E^2}{E-E_t\nu^2} & 0 \\ 0 & 0 & \frac{\beta E}{2(1+\nu)} \end{bmatrix} \tag{26}$$

This is the stiffness matrix which Bažant and Oh[7] obtained when they inverted their compliance relation for partly cracked concrete. The only difference lies in the fact that we have included a shear term, whereas they elaborated their equations in the principal stress space.

Our model can also be related to the well-known two-orthogonal crack models[16], in which secondary cracks are allowed to form only orthogonal to primary cracks. To demonstrate this, we consider two orthogonal cracks aligned with the coordinate axes. For such a system the transformation matrix $\mathbf{N}$ reads:

$$\mathbf{N} = \begin{bmatrix} 1 & 0 & 0 & 0 \\ 0 & 0 & 1 & 0 \\ 0 & 1 & 0 & -1 \end{bmatrix} \tag{27}$$

Invoking relation (23) for the concrete, we may derive that:

$$\mathbf{N}^{T}\mathbf{D}^{co}\mathbf{N} = \frac{E}{1-\nu^2}\begin{bmatrix} 1 & 0 & \nu & 0 \\ 0 & \frac{1}{2}(1-\nu) & 0 & -\frac{1}{2}(1-\nu) \\ \nu & 0 & 1 & 0 \\ 0 & -\frac{1}{2}(1-\nu) & 0 & \frac{1}{2}(1-\nu) \end{bmatrix} \tag{28}$$

so that:

$$(\mathbf{D}^{cr}+\mathbf{N}^{T}\mathbf{D}^{co}\mathbf{N})^{-1} =$$

$$\frac{1}{E}\begin{bmatrix} 1 & 0 & -\nu & 0 \\ 0 & 2\frac{(1-\beta)(1+\nu)}{\beta(2-\beta)} & 0 & 2\frac{(1-\beta)^2(1+\nu)}{\beta(2-\beta)} \\ -\nu & 0 & 1 & 0 \\ 0 & 2\frac{(1-\beta)^2(1+\nu)}{\beta(2-\beta)} & 0 & 2\frac{(1-\beta)(1+\nu)}{\beta(2-\beta)} \end{bmatrix} \tag{29}$$

Premultiplying with $\mathbf{D}^{co}\mathbf{N}$ and postmultiplying with $\mathbf{N}^{T}\mathbf{D}^{co}$ and subtracting the result from $\mathbf{D}^{co}$ now yields:

$$\mathbf{D}^{co} - \mathbf{D}^{co}\mathbf{N}(\mathbf{D}^{cr}+\mathbf{N}^{T}\mathbf{D}^{co}\mathbf{N})^{-1}\mathbf{N}^{T}\mathbf{D}^{co} =$$

$$\begin{bmatrix} 0 & 0 & 0 \\ 0 & 0 & 0 \\ 0 & 0 & \frac{\beta E}{2(2-\beta)(1+\nu)} \end{bmatrix} \tag{30}$$

It is noted that the factor $\beta/(2-\beta)$ which reduces the shear stiffness of the cracked system now does not equal the usual shear retention factor. This is because the factor $\beta/(1-\beta)$ which has been inserted in the stiffness matrix for the cracks $\mathbf{D}^{cr}$, has been derived under the assumption that there is only one crack. Indeed, if we assume that there are two cracks, so that the total strain is composed of the concrete strain and the strains of two cracks, we may

derive that the reduction factor for each crack should be taken equal to $2\beta/(1-\beta)$ as to ensure that the shear stiffness of the total system is equal to $\frac{1}{2}\beta E/(1+\nu)$. However, the difference is not great as is shown in *Figure 3*, so that the results which we obtain if we force the cracks to form orthogonal, are close to answers obtained by the common two-orthogonal crack models.

In a similar manner, relations can be elaborated with some other non-orthogonal crack models[17-19], although the derivations are usually somewhat more tedious and cumbersome.

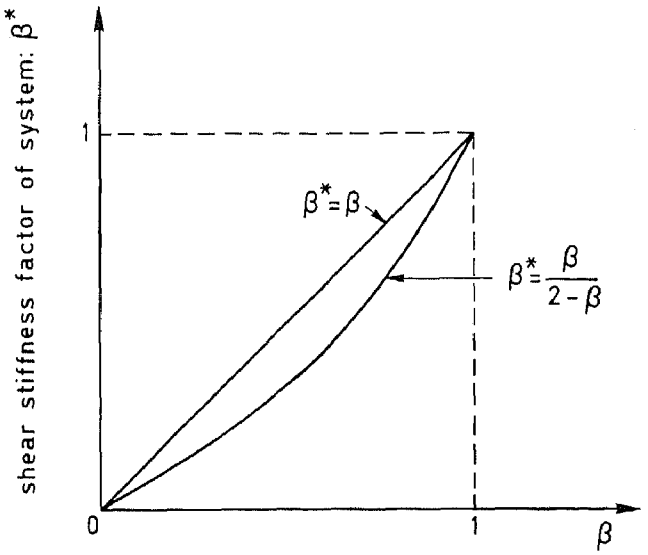

Figure 3 Shear stiffness of cracked concrete as a function of the shear retention factor β for two cracks in an integration point

BEAM FAILING IN SHEAR

The first example which we consider is the moderately deep beam of *Figure 4*. This beam has been tested experimentally[27] and has been analysed using the DIANA finite element program[28], in which the procedures described in the foregoing have been implemented. The properties of the concrete were assumed to be: Young's modulus $E_c = 28{,}000$ N/mm^2, Poisson's ratio $\nu = 0.2$, tensile strength $f_{ct} = 2.5$ N/mm^2, shear retention factor $\beta = 0.08$ and fracture energy $G_f = 0.06$ N/mm. The beam had a thickness of 200 mm and had no shear reinforcement as is shown in *Figure 5*. The reinforcement at the bottom of the beam had a Young's modulus $E_s = 210{,}000$ N/mm^2 and a yield stress $\sigma_y = 440$ N/mm^2.

The analysis was carried out using eight-noded Serendipity plane stress elements with nine-point Gaussian integration. It has been argued[40] that it may be favourable to use Lobatto integration as such a closed scheme better accounts for the bending influence. In that publication it was also asserted that it is sometimes better to employ triangular elements as they do not suffer from directional bias which may also cause spurious cracking. The importance of these aspects will be investigated in future and a particular aspect concerning the order of numerical integration is addressed in the next section.

In the experiment, it was observed that failure occurred due to the diagonal cracks shown in *Figure 7*. Prior to the development of the diagonal cracks, vertical cracks had arisen predominantly in the constant moment zone. In the numerical analysis we also observe that vertical cracks due to bending arise first. On subsequent loading the stresses rotate and new, non-vertical crack form in the

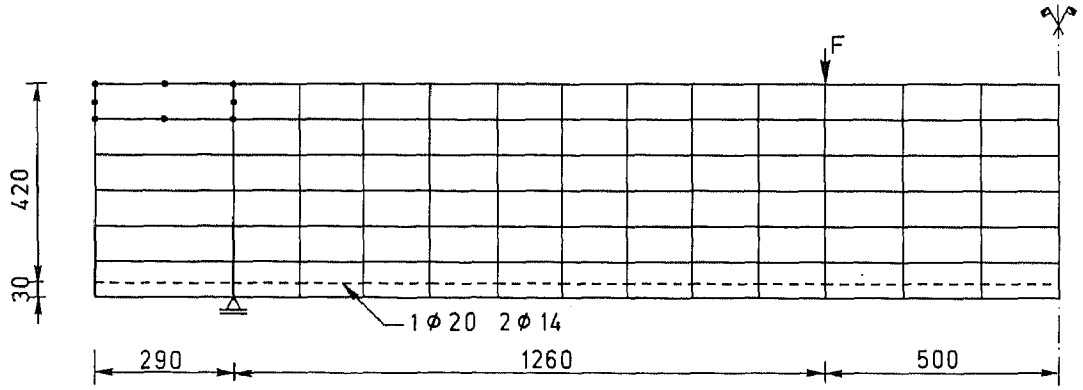

Figure 4 Finite element mesh for moderately deep beam

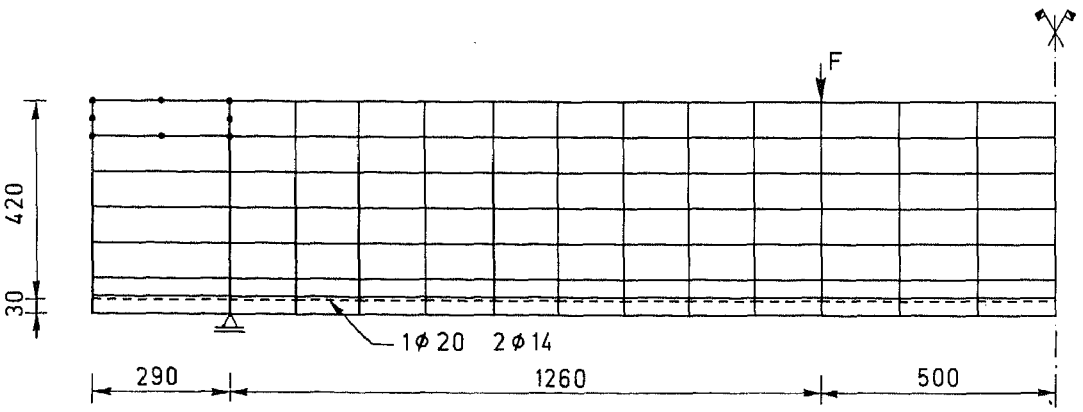

Figure 5 Refined mesh for moderately deep beam

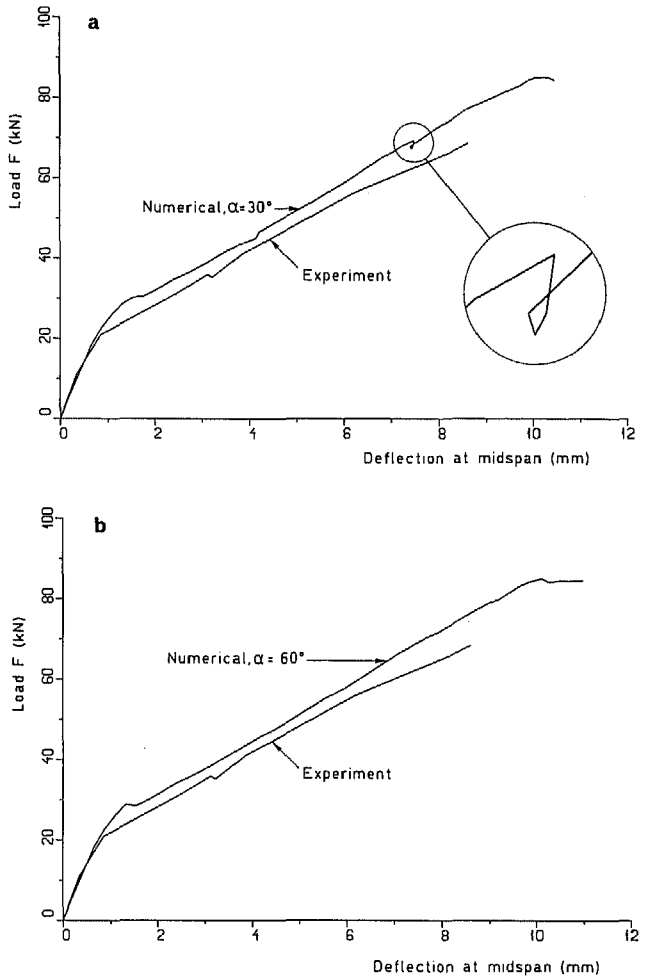

Figure 6 Load *versus* deflection at midspan for the beam problem, (a) $\alpha=30°$, (b) $\alpha=60°$

region between the point load and the support (see *Figures 8* and *9*). Some of these cracks arise in integration points in which a vertical crack already existed. This phenomenon can be handled with the present model as has also been verified by combined tension-shear loadings on panels in a homogeneous state of stress. Yet, allowing cracks to form every time the stresses rotate slightly and violate the tensile strength in the new principal direction, leads to excessive formation of new cracks and closing of existing cracks. Therefore a threshold angle α has been adopted which allows new cracks to form in an integration point only when the angle between the principal stress direction and the normal to the existing crack has exceeded the threshold angle.

The first analyses with the model were carried out using a relatively high threshold angle, namely $\alpha=60°$, which information was accidentally omitted in a previous publication[15]. To investigate the performance of the model for lower values of α, other analyses have been performed using a threshold value of 30°. The impact on the global load–displacement curve of *Figures 6a* and *6b* appeared negligible until a displacement at midspan of 7.2 mm. Then, the analysis with $\alpha=30°$ (*Figure 6a*) diverged. No convergence could be achieved no matter how small the imposed displacement increments were taken. However, when we decremented displacements we were able to get a converged solution, although a number of new cracks arose. When we observed no more physical changes we again incremented displacements and we could continue the solution up to and beyond the point where the steel started yielding.

It is debatable whether the 'snap-back' behaviour of *Figure 6a* is physical or merely numerical. Spurious non-physical solutions have for instance been observed in fluid mechanics which appeared to vanish on mesh refine-

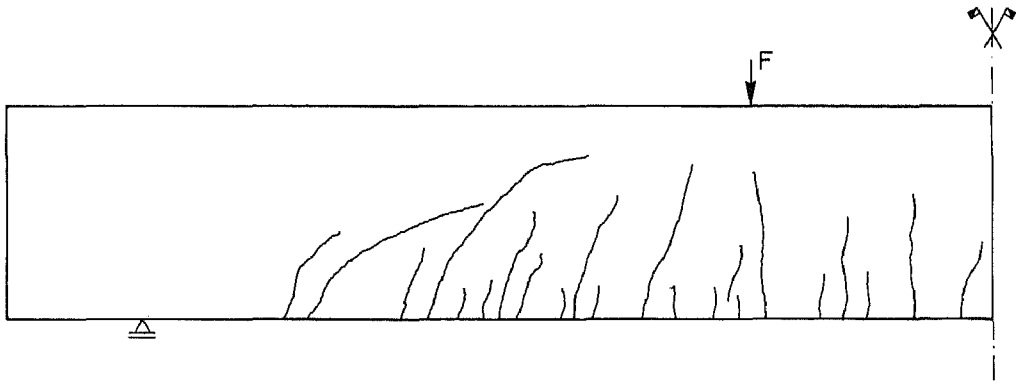

Figure 7 Experimentally observed crack pattern at impending failure

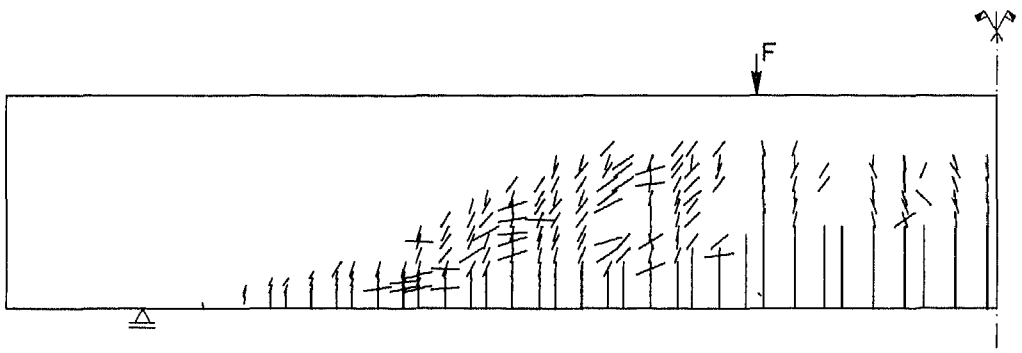

Figure 8 Calculated crack pattern at impending failure for high threshold angle (all cracks)

ment[29]. This observation would support the conclusion that the observed behaviour is numerical rather than physical. Indeed, when we recalculated this problem with a mesh which was slightly refined near the location of the reinforcement (*Figure 5*), no numerical difficulties were met at this point. Yet, convergence was slow also in this case and small steps had to be taken.

Although the behaviour is thought to be non-physical in the present case, it has been shown that snap-backs are possible when employing softening models[30]. It is therefore not unthinkable that numerical difficulties which we meet at such points will be the starting point of a descending branch on the load–displacement curve and of a 'brittle failure' if we include a more accurate relation between the shear stress and the shear strain in a crack.

As in most smeared crack analyses a certain degree of diffusion in the crack pattern is observed (see *Figures 8* and *9*). This diffused crack pattern largely disappears when we plot only those cracks which carry no normal stress, which may be interpreted as micro-cracks which have coalesced into one macro-crack. Then the crack patterns of *Figures 10* and *11* are obtained, which clearly exhibit strain localization including the initiation of a diagonal crack. This diagonal crack is closer to the point load for the low threshold angle, while it is more near the support for the higher threshold angle. A similar trend was observed for computations on this beam upon the introduction of a variable shear retention factor[31]. It seems that the use of a very low value for the shear retention factor forces the diagonal crack to move to the point load, where it is recalled that although both calculations reported here have been performed using the same shear retention factor, the shear capacity for the calculation with the lower threshold angle is effectively lower because of the existence of more multiply cracked integration points (see *Figure 3*).

The examples presented in this section and also those which we will show in the next section have been obtained using secant and quasi-Newton methods[32,33]. They could not be obtained using a standard Newton–Raphson method as with this type of method convergence (energy criterion $\varepsilon = 0.0001$) could not be achieved at various stages of the loading process. Secant and quasi-Newton methods are very competing when analysing concrete

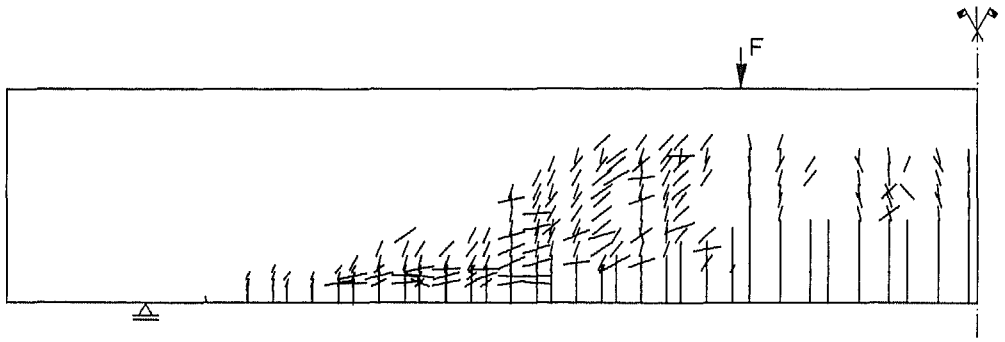

Figure 9 Calculated crack pattern at impending failure for lower threshold angle (all cracks)

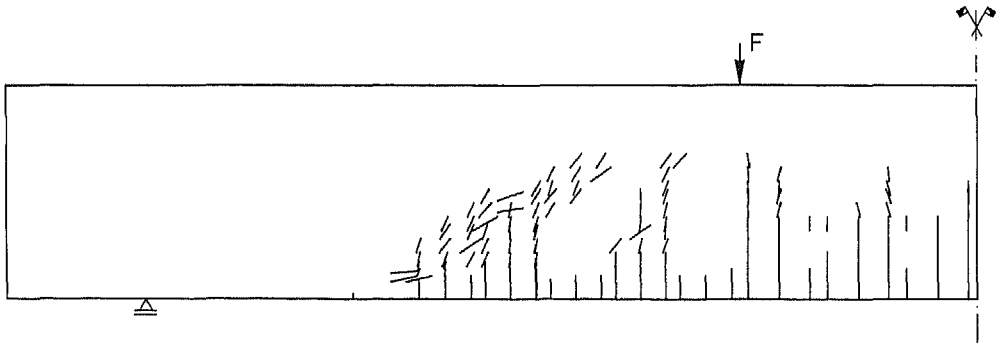

Figure 10 Cracks that transfer no normal stress at impending failure for high threshold angle

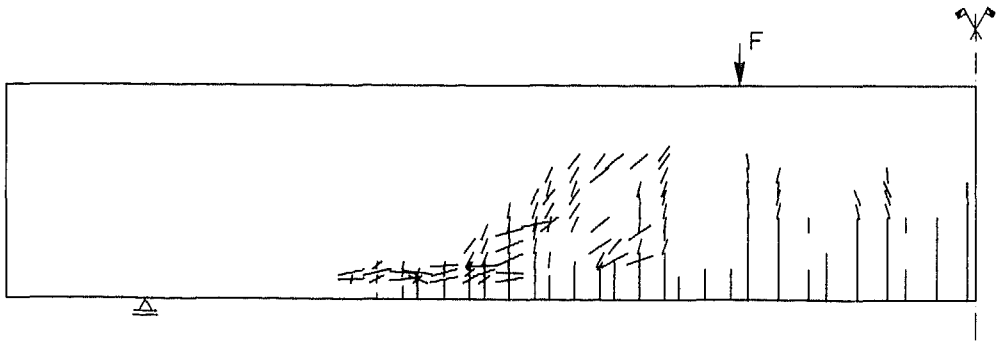

Figure 11 Cracks that transfer no normal stress at impending failure for lower threshold angle

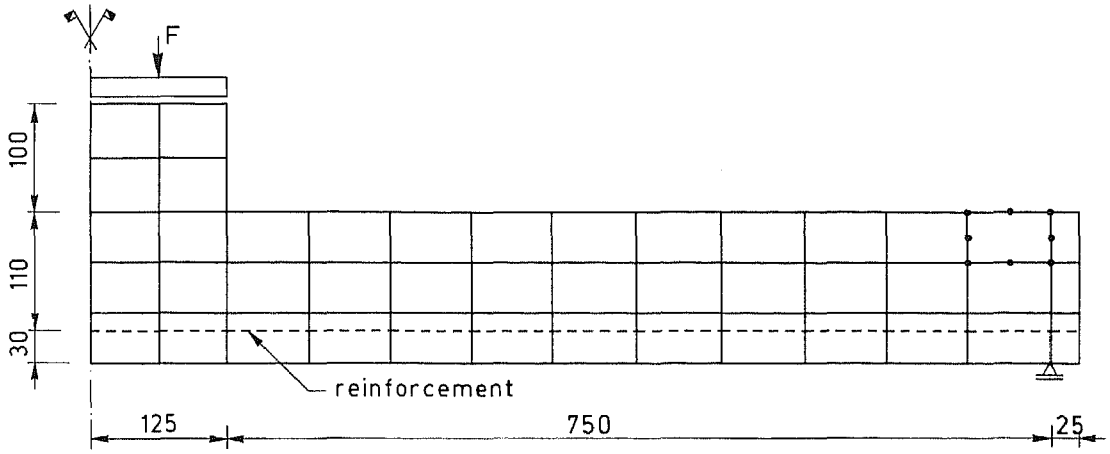

Figure 12 Coarse mesh for axisymmetric slab

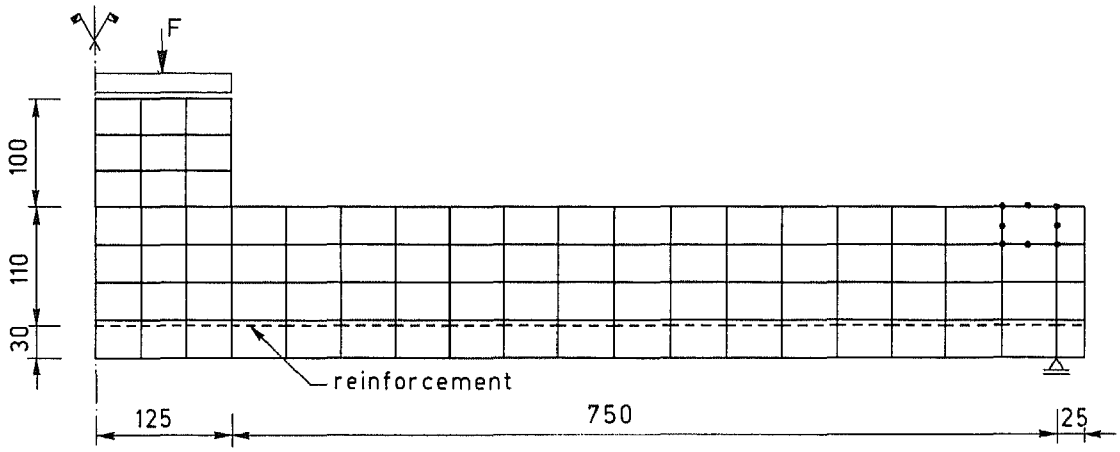

Figure 13 Finer mesh for axisymmetric slab

structures under displacement control[33]. Analyses of concrete structures with these methods under arc-length control are sometimes less successful, which prompted the development of a line-search procedure in conjunction with arc-length control[34]. Then economic analyses are feasible again. Indeed, the snap-back behaviour which we encountered could have been analysed more elegantly using an arc-length technique as was done by Crisfield for another snap-back problem in a concrete beam[35].

It is remarked finally that no attempt has been made to accurately fit the experimental load–displacement curve. Instead, we have focused on simulating the basic characteristics of this problem such as the inception of a dominant diagonal crack and the brittle failure.

PUNCHING SHEAR OF AN AXISYMMETRIC SLAB

The second example that we consider is the axisymmetric slab of *Figures 12* and *13*. The properties of the concrete are now given by: Young's modulus $E_c = 28{,}000$ N/mm^2, Poisson's ratio $\nu = 0.2$, tensile strength $f_{ct} = 2.6$ N/mm^2, shear retention factor $\beta = 0.2$, fracture energy $G_f = 0.06$ N/mm, cohesion $c = 9.6$ N/mm^2, friction angle $\phi = 30°$. The slab is reinforced isotropically with a reinforcement ratio of 1% and the properties of the reinforcement are $E_s = 205{,}000$ N/mm^2 and $\sigma_y = 465$ N/mm^2. The experimental failure mechanism of this slab is ultimately due to punching shear[36]. Earlier

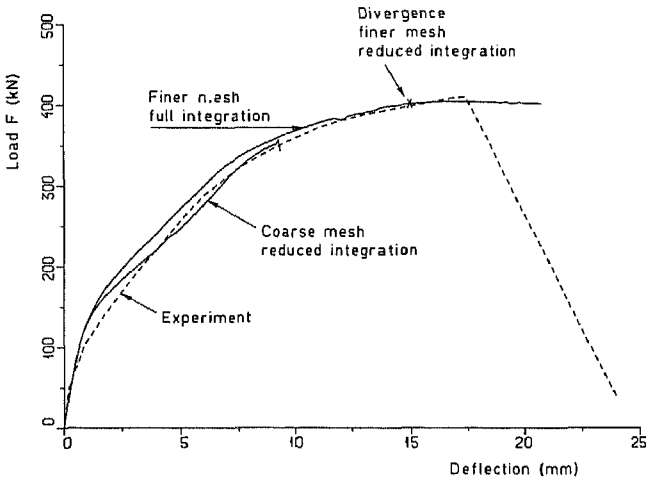

Figure 14 Load–deflection curves for axisymmetric slab

analyses of this slab had to be stopped after an imposed displacement of approximately 7 mm[37] or involved only crack formation[15].

The first analysis involving both plasticity and crack formation was carried out for the coarse mesh of *Figure 12* and reduced four-point Gaussian integration was employed. After incrementing the displacement up to a deflection of 9.6 mm no convergence appeared possible although very small displacement increments were imposed (see *Figure 14*). However, when the analysis was

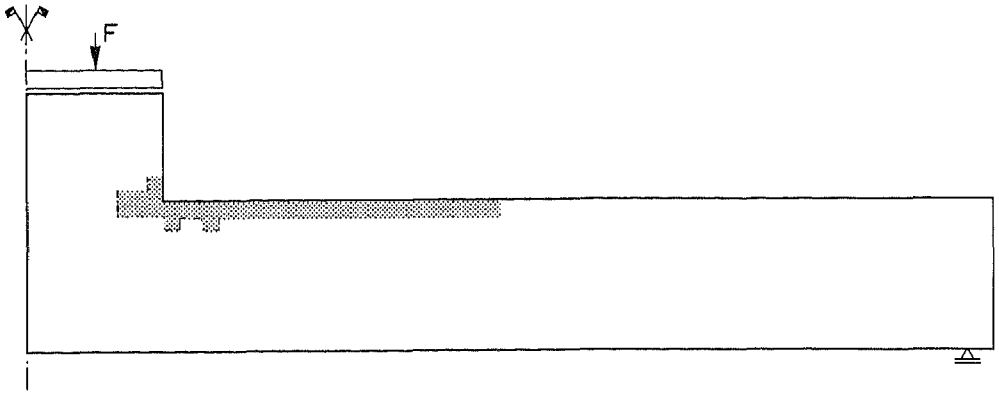

Figure 15 Plastic region at peak load level (shaded)

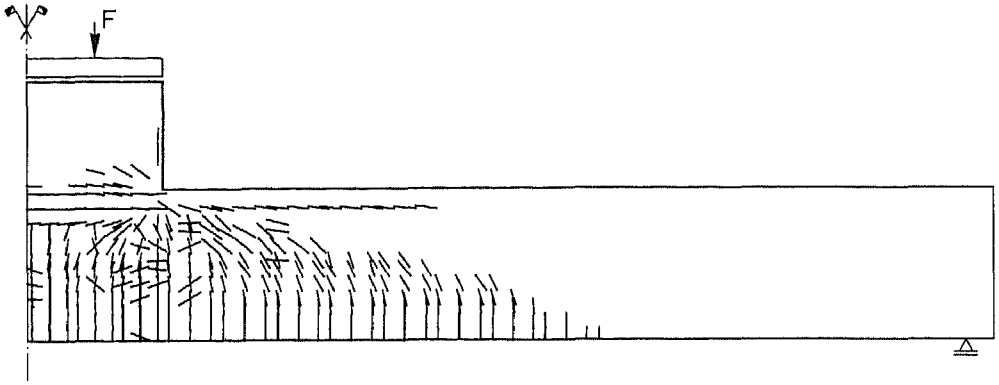

Figure 16 Tangential crack pattern at peak load level

repeated with exactly the same mesh and the same material parameters, but with 'full' nine-point integration, displacements could be imposed until and beyond a plateau in the load–displacement curve had been reached. The same trend was observed for computations with the refined mesh of *Figure 13*, i.e. the analysis with 'full' integration could be continued after the plateau had been reached and the analysis with reduced integration diverged at some displacement level (*Figure 14*). Yet, the latter calculation with 'reduced' integration could be continued much further than the computation with 'reduced' integration for the coarser mesh. This would again indicate that spurious snap-backs and divergence gradually disappear with mesh refinement.

The poor behaviour of 'reduced' integration in conjunction with crack formation has been explained to be caused by the introduction of spurious zero-energy modes upon the formation of cracks in 'reduced' integrated elements[38]. With the formation of a new crack, an extra spurious zero-energy mode is introduced, so that we have four additional zero-energy modes when all four integration points are cracked. Observations about incorrect predictions of structural behaviour when using reduced integration have also been reported by Crisfield[35], but it has not yet been demonstrated that it may even lead to divergence of the iterative procedure. This example clearly illustrates that associating divergence of the iterative procedure with structural failure which is sometimes done especially with 'brittle failures' may be misleading. It is the authors' opinion that this is incorrect and that a proper assessment of the structural behaviour can only be made if the entire load–deflection curve can be traced.

The load–deflection curve of *Figure 14* ultimately reaches a plateau. Usually such a plateau is identified with yielding of the reinforcement. In this example this was not the case as yielding started only after a deflection of approximately 20 mm, thus after that a considerable part of the plateau had been traversed. Probably, the plateau is due to yielding of the concrete in the compression zone (see *Figure 15*). If we had included a softening model for the concrete in compression instead of a perfectly-plastic model, we would presumably have observed a softening behaviour instead of a plateau. Inclusion of such a softening model and a non-constant shear retention factor for the cracks seem important refinements on the constitutive model in order to obtain a post-peak softening response.

The tangential crack pattern of *Figure 16* that we calculated at peak load is very shallow. This is in accordance with the experimental observations which also show that tangential cracking spreads over a rather large area[36]. The observation that radial cracks arise almost throughout the slab already in an early stage of the loading process is also in agreement with experimental findings (*Figure 18*). When we plot only the so-called major cracks which carry no more tensile stress, we again observe a much more localized pattern which reveals the initiation of a diagonal shear crack (see *Figure 17*). The large horizontal crack that we also observe in *Figure 17* is somewhat strange as such cracks are not reported from tests on such specimens. At first, it was assumed that these horizontal cracks were caused by the modelling of the boundary conditions as the area where the loading was applied was forced to remain plane because of the adopted

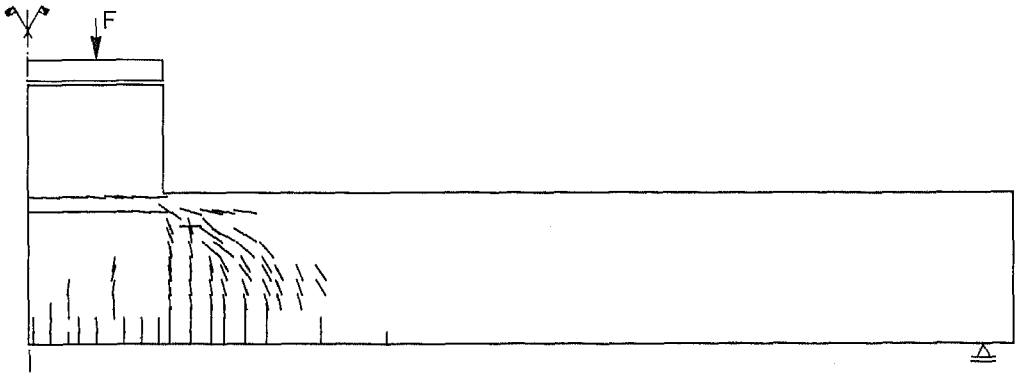

Figure 17 Major cracks (no normal stress transfer) at peak load

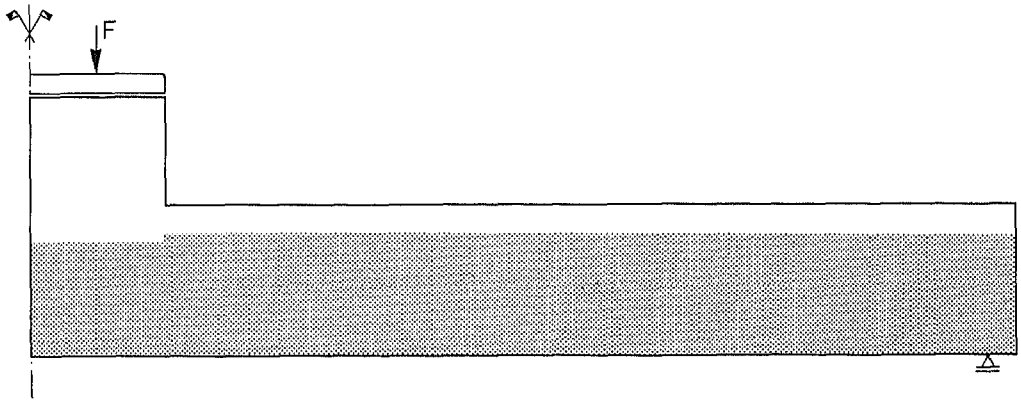

Figure 18 Region in which radial cracks have developed (shaded)

displacement control. In the experiment, some load-distributing medium was applied so that the boundary conditions are more like a uniform traction. Nevertheless, when the analysis was repeated for a uniform traction and using an arc-length method to control the loading process, the same cracks were observed. Indeed, on a closer examination of the experimental data, it appeared that it may well be possible that such cracks really arise[36].

A final remark concerns the threshold angle α for the formation of secondary and eventually of tertiary cracks. The results presented in this section have been obtained using a threshold angle of 60°. An analysis with $\alpha = 30°$ has also been undertaken, but the solution appeared to be rather unstable, involving several snap-backs and snap-throughs, probably of a numerical nature. On closer examination a number of integration points were detected in which no less than four cracks had arisen (one radial and three tangential cracks). It may be expected that little (shear) stiffness remains and that spurious zero-energy modes may easily occur in such points thus leading to ill-conditioning. Apparently the slab problem is significantly more difficult than the beam problem of the preceding section for which an analysis with $\alpha = 30°$ was feasible.

CONCLUSIONS

A new smeared crack model which permits non-orthogonal cracks has been described. It is transparent as the strain increment is divided into a concrete and into a crack strain increment. It can be related to other smeared models which are used to simulate crack formation and some relations have been elaborated.

This decomposition moreover allows for a natural combination of crack formation and other non-linear phenomena such as plasticity and creep and with thermal dilation and shrinkage within a smeared finite element model[15,20]. A numerical algorithm that handles the combination of plasticity and crack formation has been discussed in somewhat greater detail.

The use of so-called reduced integration in conjunction with crack formation may lead to erroneous results and to divergence of the iterative procedure. This observation is in line with statements in some other publications[35,38]. When using eight-noded elements three-by-three or 'full' Gauss integration is more reliable for concrete structures as this largely prevents spurious zero-energy modes to occur.

It is incorrect to identify structural failure with divergence of the iterative procedure as is sometimes done for brittle failures. This has been demonstrated by the example of an axisymmetric slab which diverged entirely because a reduced integration scheme had been employed. For a proper assessment of the structural behaviour it is necessary to trace the post-failure response also. This may involve analysing snap-through and snap-back behaviour for which the arc-length method seems very suitable also for concrete structures[34]. An example thereof has been discussed, although it is doubted whether the observed snap-back behaviour is of a physical nature.

Smeared crack approaches are capable of predicting dominant diagonal cracks which occur in shear failures. Reasonable crack patterns for a beam and for an axi-symmetric slab both failing in shear, were obtained despite a certain degree of diffusion. So, strain-localization can to a certain extent be represented by smeared crack models. Here, the situation is similar to

non-associated plasticity, where the localization of deformation in thin shear bands can also be predicted by smeared representations[22,41].

ACKNOWLEDGEMENT

The research described in this paper was assisted financially by CUR-Committee A26 'Concrete Mechanics' and by the Section 'Bouwspeurwerk' of the Department of Public Works.

NOMENCLATURE

- α threshold angle
- β shear retention factor
- γ shear strain
- ϕ friction angle
- ε strain
- θ inclination angle
- ν Poisson's ratio
- σ stress

REFERENCES

1 Ngo, D. and Scordelis, A. C. Finite element analysis of reinforced concrete beams, *J. Am. Concrete Inst.*, **64**, 152–163 (1967)
2 Nilson, A. H. Non-linear analysis of concrete by the finite element method, *J. Am. Concrete Inst.*, **65**, 757–766 (1968)
3 Saouma, V. E. and Ingraffea, A. R. Fracture mechanics analysis of discrete cracking, in *Final Report IABSE Colloq. Adv. Mech. Reinforced Concrete*, Delft University Press, Delft, 413–436 (1981)
4 Grootenboer, H. J. Finite element analysis of two-dimensional reinforced concrete, taking account of nonlinear physical behaviour and the development of discrete cracks, *Dissertation*, Delft University of Technology, Delft (1979)
5 Rashid, Y. R. Analysis of prestressed concrete pressure vessels, *Nucl. Eng. Design*, **7**, 334–344 (1968)
6 Suidan, M. and Schnobrich, W. C. Finite element analysis of reinforced concrete, *ASCE J. Struct. Div.*, **99**, 2109–2122 (1973)
7 Bažant, Z. P. and Oh, B. Crack band theory for fracture of concrete, *RILEM Mat. Struct.*, **16**, 155–177 (1983)
8 Nilsson, L. and Oldenburg, M. Nonlinear wave propagation in plastic fracturing materials—a constitutive modelling and finite element analysis, in *Proc. IUTAM Symp. Nonlinear Deformation Waves* (Eds. U. Nigul and J. Engelbrecht), Springer, Berlin–Heidelberg, 209–217 (1983)
9 Rots, J. G., Kusters, G. M. A. and Blaauwendraad, J. The need for fracture mechanics options in finite element models for concrete structures, in *Proc. Int. Conf. Computer Aided Analysis and Design of Concrete Structures* (Eds. F. Damjanic *et al.*), Pineridge Press, Swansea, Part 1, 19–32 (1984)
10 Cope, R. J., Rao, P. V., Clark, L. A. and Norris, P. Modelling of reinforced concrete behaviour for finite element analysis of bridge slabs, in *Numerical Methods for Non-Linear Problems* (Eds. C. Taylor, E. Hinton and D. R. J. Owen), Pineridge Press, Swansea, Vol. 1, 457–470 (1980)
11 Cope, R. J. and Rao, P. V. Non-linear finite element strategies for bridge slabs, in *Final Report IABSE Colloq. Adv. Mech. Reinforced Concrete*, Delft University Press, Delft, 273–288 (1981)
12 Bažant, Z. P. Discussion on Session 2, Structural modelling for numerical analysis, in *Final Report IABSE Colloq. Adv. Mech. Reinforced Concrete*, Delft University Press, Delft, 482 (1981)
13 Bažant, Z. P. Comment on orthotropic models for concrete and geomaterials, *ASCE J. Eng. Mech. Div.*, **109**, 849–864 (1983)
14 Milford, R. V. and Schnobrich, W. C. Numerical model for cracked reinforced concrete, in *Proc. Int. Conf. Computer Aided Analysis and Design of Concrete Structure* (Eds. F. Damjanic *et al.*), Pineridge Press, Swansea, Part 1, 71–84 (1984)
15 de Borst, R. and Nauta, P. Smeared crack analysis of reinforced concrete beams and slabs failing in shear, in *Proc. Int. Conf. Computer Aided Analysis and Design of Concrete Structures* (Eds. F. Damjanic *et al.*), Pineridge Press, Swansea, Part 1, 261–273 (1984)
16 Nilson, A. H. *et al.* State-of-the-art report on *Finite Element Analysis of Reinforced Concrete*, ASCE, New York (1982)
17 Litton, R. W. A contribution to the analysis of concrete structures under cyclic loading, *Dissertation*, University of California, Berkeley (1976)
18 Kristjansson, R. Physikalisch und geometrisch nichtlineare Berechnung von Stahlbetonplatten mit Hilfe Finiter Elemente, *Dissertation*, Technische Hochschule Darmstadt, Darmstadt (1977)
19 Ebbinghaus, P. Herleitung eines Verfahrens zur Berechnung von Stahlbetonscheiben unter Berücksichtigung der Rissentwicklung, *Dissertation*, Rheinisch-Westfälische Technische Hochschule, Aachen (1975)
20 Bažant, Z. P. and Chern, J. C. Concrete creep at variable humidity, *Report No. 84-5/665c*, Center for Concrete and Geomaterials, The Technological Institute, Northwestern University (1984)
21 van Mier, J. G. M. Complete stress–strain behaviour and damaging status of concrete under multiaxial conditions, in *Proc. RILEM/CEB Symp. Concrete under Multiaxial Conditions, Toulouse*, 75–85 (1984)
22 Vermeer, P. A. and de Borst, R. Non-associated plasticity for soils, concrete and rock, *Heron*, **29** (3), 1–64 (1984)
23 Vermeer, P. A. A modified initial strain method for plasticity problems, in *Proc. 3rd Int. Conf. Num. Meth. Geomech.* (Ed. W. Wittke), Balkema, Rotterdam, 377–387 (1979)
24 de Borst, R. Implicit integration of stress–strain laws in thermoplasticity, *TNO-IBBC Report No. BI-84-43*, Rijswijk (1984)
25 Cope, R. J. personal communication (1984)
26 Reinhardt, H. W. and Cornelissen, H. A. W. Post-peak cyclic behaviour of concrete in uniaxial tensile and alternating tensile and compressive loading, *Cement Concrete Res.*, **14**, 263–270 (1984)
27 Walraven, J. C. The influence of depth on the shear strength of lightweight concrete beams without shear reinforcement, *Report 5-78-4*, Stevin Laboratory, Delft University of Technology, Delft (1978)
28 de Borst, R., Kusters, G. M. A., Nauta, P. and de Witte, F. C. DIANA, a three-dimensional, nonlinear finite element package on a microcomputer, in *Engineering Software for Microcomputers* (Eds. B. A. Schrefler, R. W. Lewis and S. A. Odorizzi), Pineridge Press, Swansea, 435–446 (1984)
29 Azmy, Y. Y. and Dorning, J. J. Arc-length continuation of nodal integral method solutions to the non-linear Navier–Stokes equations, in *Numerical Methods for Non-linear Problems* (Eds. C. Taylor, E. Hinton, D. R. J. Owen and E. Oñate), Pineridge Press, Swansea, Vol. 2, 672–687 (1984)
30 Crisfield, M. A. Local instabilities in the non-linear analysis of reinforced concrete beams and slabs, *Proc. Inst. Civ. Eng.*, Part 2, **73**, 135–145 (1982)
31 Rots, J. G., Kusters, G. M. A. and Nauta, P. Variable reduction factor for shear resistance of cracked concrete, *TNO-IBBC Report BI-84-33*, Rijswijk (1984) (in Dutch)
32 Crisfield, M. A. Accelerated solution techniques and concrete cracking, *Comput. Meth. Appl. Mech. Eng.*, **33**, 585–607 (1982)
33 de Borst, R. Application of advanced solution techniques to concrete cracking and non-associated plasticity, in *Numerical Methods for Non-linear Problems* (Eds. C. Taylor, E. Hinton, D. R. J. Owen and E. Oñate), Pineridge Press, Swansea, Vol. 2, 314–325 (1984)
34 Crisfield, M. A. An arc-length method including line-searches and accelerations, *Int. J. Num. Meth. Eng.*, **19**, 1269–1289 (1983)
35 Crisfield, M. A. Difficulties of current numerical models for reinforced-concrete and some tentative solutions, in *Proc. Int. Conf. Computer Aided Analysis and Design of Concrete Structures* (Eds. F. Damjanic *et al.*), Pineridge Press, Swansea, Part 1, 331–358 (1984)
36 Walraven, J. C. personal communication (1984)
37 van Foeken, R. J. Prediction of crack patterns and load-deflection curves of some reinforced concrete benchmark problems with DIANA, *TNO-IBBC Report BI-83-40*, Rijswijk (1983)
38 Dodds, R. H., Darwin, D., Smith, J. L. and Leibengood, L. D. Grid size effects with smeared cracking in finite element analysis of reinforced concrete, *SM Report No. 6*, University of Kansas, Lawrence, Kansas (1982)
39 Mehlhorn, G. On the application of the finite element method for analysing reinforced concrete plates and planar structures—a survey of some research activities by the Darmstadt group, in *Final Report IASS Symp. Nonlinear Behaviour of Reinforced Concrete Spatial Structures* (Eds. G. Mehlhorn, H. Rühle and W. Zerna), Werner-Verlag, Düsseldorf, Vol. 3, 159–190 (1978)
40 Bergan, P. Some aspects of interpolation and integration in non-linear finite element analysis of reinforced concrete structures, in *Proc. Int. Conf. Computer Aided Analysis and Design of Concrete Structures* (Eds. F. Damjanic *et al.*), Pineridge Press, Swansea, Part 1, 301–316 (1984)
41 de Borst, R. and Vermeer, P. A. Possibilities and limitations of finite elements for limit analysis, *Géotechnique*, **34**, 199–210 (1984)